Lubrication analysis of thermocapillary-induced nonwetting

Loren B. S. Sumner[a)]
Department of Mechanical and Industrial Engineering, Mercer University, Macon, Georgia 31207

Andrea M. Wood and G. Paul Neitzel
G. W. Woodruff School of Mechanical Engineering, Georgia Institute of Technology, Atlanta, Georgia 30332

(Received 7 March 2003; accepted 22 July 2003; published 2 September 2003)

Recent interest in the phenomenon of thermocapillary-induced noncoalescence and nonwetting has produced experimental evidence of the existence of a film of lubricating gas that prevents the two surfaces in question (liquid–liquid for noncoalescence; liquid–solid for nonwetting) from coming into contact with one another. Measurements further indicate that the pressure distribution in this film creates a dimpled liquid free-surface. Lubrication theory is employed to investigate the coupled effects of liquid and gas flows for a two-dimensional nonwetting case of a hot droplet pressed toward a cold wall. The analysis focuses on the respective roles of viscous and inertial forces on droplet deformation. Resultant droplet shapes show an influence of gas viscosity maintaining nonwetting and of inertia contributing to a dimple. Previous analyses of thermocapillary-driven flow in liquid layers and droplets model the gas as purely passive which cannot be the case in the present application. © *2003 American Institute of Physics.* [DOI: 10.1063/1.1608940]

I. INTRODUCTION

The sustainment of a state of permanent noncoalescence between two bodies of the same liquid or nonwetting of a solid normally wetted by a particular liquid is a relatively new area of investigation within fluid mechanics. Although examples of transient noncoalescence (e.g., bouncing and floating water droplets) date back to the work of Rayleigh[1–3] and Reynolds,[4] it is the permanent variety—in particular, that driven by thermocapillarity—that concerns us here. This phenomenon occurs when the two surfaces attempting to be brought together are at sufficiently different temperatures. Thermocapillary convection, driven by the temperature dependence of surface tension, exists not only in the liquid(s) experiencing a surface-temperature gradient, but also in the surrounding gas through viscous action such that, under the proper set of conditions, gas is driven into the space between the surfaces, forming a lubrication film that keeps the liquid–liquid or liquid–solid surfaces sufficiently apart that attractive van der Waals forces remain weak.

The first systematic experiments investigating permanent, thermocapillary-induced noncoalescence were performed by Dell'Aversana *et al.*[5] Subsequent work[6] verified directly, using interferometry, the existence of a lubricating gas film of order microns in thickness for droplets of order millimeters in size (noncoalescence has been observed for droplets an order of magnitude larger than this). Accurate measurements of film thickness for the case of nonwetting reveal a dimple, an area of reversed curvature, in the liquid surface having a symmetric shape about the center of the droplet. Additional discussion of various aspects of the phenomena may be found in the short article by Dell'Aversana and Neitzel[7] and in a pair of papers by Monti *et al.*[8,9] A more comprehensive review of both permanent and temporary noncoalescence and nonwetting may be found in the recent review article of Neitzel and Dell'Aversana.[10]

Theoretical treatment of thermocapillary noncoalescence and nowetting is complicated by the disparity of length scales involved. As mentioned in the previous paragraph, droplets of millimeter (or larger) size generate gas films of micron-sized thickness. Because the gas plays a central role in the process, it may not be neglected, particularly if one is interested in simulating accurately the free-surface shape. It is the interaction between the liquid and gas through the normal-stress boundary condition that determines this shape. Monti *et al.*[8,9] computed thermocapillary convection within a droplet whose shape was fixed by static considerations, using the surface speeds obtained to calculate flow in the surrounding gas. The computed pressure distribution in the gas film indicates a high pressure in the center that could give rise to a dimple, but the free-surface position was not recalculated in light of this.

The present work adopts an alternate approach using lubrication theory to simultaneously determine the coupled flows in the liquid and gas for a two-dimensional (2-D) nonwetting situation of a hot liquid droplet pressed against a cold solid surface; 2-D noncoalescence and nonwetting have been demonstrated experimentally by Nalevanko,[11] so the problem is of practical interest. The flow in the gas film, with its small thickness-to-length (aspect) ratio, is clearly a candidate for lubrication theory; its application to the flow in the liquid phase implies the assumption of a thin, nearly flat droplet.

There are several examples in the literature of the application of lubrication theory to problems involving thermocapillary convection. Sen and Davis[12] performed such an analysis for 2-D flow in a slot bounded by differentially heated endwalls; this work was later extended by Sen.[13] Ehrhard and Davis[14] studied the influence of thermocapillary

a)Author to whom all correspondence should be addressed. Electronic mail: sumner_lb@mercer.edu

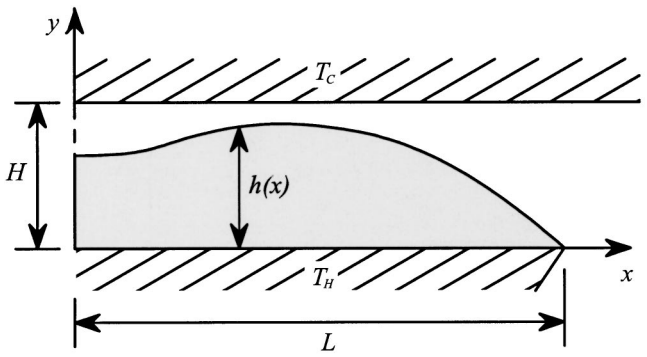

FIG. 1. Problem domain and boundaries.

convection on the inhibition or promotion of spreading on heated and cooled plates. Benintendi and Smith[15] used the Ehrhard and Davis formulation to examine the effects of slip coefficient and mobility capillary number on non-isothermal spreading. Smith[16] likewise used lubrication theory to study the migration of a thin droplet along a differentially heated surface. In all of these applications, the gas bounding the liquid free-surface was regarded as passive since it plays no central role in the flow under consideration.

In the related problem of Marangoni convection due to thermocapillarity experienced by liquid layers heated from below, experiments by Van Hook *et al.*[17] on the initiation of long-wave instabilities were unable to be explained with a so-called ''single-layer'' model considering the liquid only. A two-layer model developed by Golovin *et al.*[18] employed a multiple-time-scale technique (with convection in both layers), while a two-layer lubrication model by Van Hook *et al.*[19] considered only conduction in the gas layer. The present work represents the first that we know of to use lubrication theory to treat analytically both the liquid and gas flows.

In the following section we present the mathematical formulation of the problem, discussing, in particular, the implications of various scaling choices. We then present results for the $O(1)$ and $O(A)$ treatments, where $A \ll 1$ is the aspect ratio in terms of which the solution is expanded. Finally, results of computations for various choices of parameters are presented and discussed.

II. MATHEMATICAL FORMULATION

Steady, two-dimensional, liquid and lubricating-gas flow fields coupled by a deformable interface are considered. Both phases are treated as incompressible, Newtonian fluids having constant material properties with the exception that the surface tension of the liquid is assumed to vary linearly with temperature. As shown in Fig. 1, the liquid is bounded below by a flat, solid surface at constant temperature T_H and above by the liquid/gas interface. The gas is bounded above by a flat, solid surface maintained at constant temperature $T_C < T_H$. Symmetry conditions are enforced on the liquid and gas flows and the interface at the center of the droplet at $x = 0$. The contact line where the interface intersects the bottom wall marks the end of the liquid droplet of length $2L$, and the gas is assumed to be open to surrounding ambient conditions, although the present formulation, focusing on the lubricating flow in and above the droplet, leaves the ambient gas flow arbitrary for $|x| > L$.

The formulation follows that of Sen and Davis[12] with the major differences attributed to our consideration of a non-passive gas and a curved leading-order interface shape subject to a non-uniform temperature gradient. The governing equations,

$$U_x + V_y = 0, \tag{1a}$$

$$\rho_g(UU_x + VU_y) = -P_x + \mu_g(U_{xx} + U_{yy}), \tag{1b}$$

$$\rho_g(UV_x + VV_y) = -P_y + \mu_g(V_{xx} + V_{yy}), \tag{1c}$$

$$U\Theta_x + V\Theta_y = \alpha_g(\Theta_{xx} + \Theta_{yy}), \tag{1d}$$

represent continuity, balance of momentum in the x and y directions (neglecting gravity), and conservation of energy in the gas; similarly

$$u_x + v_y = 0, \tag{2a}$$

$$\rho_l(uu_x + vu_y) = -p_x + \mu_l(u_{xx} + u_{yy}), \tag{2b}$$

$$\rho_l(uv_x + vv_y) = -p_y + \mu_l(v_{xx} + v_{yy}), \tag{2c}$$

$$uT_x + vT_y = \alpha_l(T_{xx} + T_{yy}), \tag{2d}$$

apply in the liquid. The dependent variables of these equations are the x and y components of velocity, U, V, and pressure P in the gas and u, v, and p in the liquid, and temperature, Θ in the gas, and T in the liquid. The properties of the fluids are the densities, ρ_g and ρ_l, viscosities μ_g and μ_l, and thermal diffusivities α_g and α_l, where g and l subscripts distinguish the gas and liquid, respectively. The boundary conditions modeling the effect of the walls, where $|x| \leqslant L$, are

$$u = v = 0, \quad T = T_H \quad (y = 0), \tag{3}$$

$$U = V = 0, \quad \Theta = T_C \quad (y = H). \tag{4}$$

Symmetry at $x = 0$ implies

$$u = v_x = T_x = 0 \quad (y \leqslant h(x)), \tag{5}$$

$$U = V_x = \Theta_x = 0 \quad (y > h(x)), \tag{6}$$

where $h(x)$ is the interface position. In index notation, interfacial boundary conditions

$$\left.\begin{aligned} [S_{ij}]_l n_j n_i - [S_{ij}]_g n_j n_i &= \sigma \mathrm{K} \\ [S_{ij}]_l n_j t_i - [S_{ij}]_g n_j t_i &= \sigma_{,i} t_i \\ \kappa_l T_{,i} n_i &= \kappa_g \Theta_{,i} n_i \\ [u_i]_l n_i &= 0 \\ [u_i]_g &= [u_i]_l \end{aligned}\right\} \quad (y = h(x)), \tag{7}$$

represent, respectively, the normal-stress, shear-stress, heat-transfer, and kinematic constraints coupling the gas and liquid flow fields, where σ is the surface tension, K denotes the interface curvature, and the thermal conductivities are indicated by κ_g and κ_l. In these equations, n_i and t_i define unit vectors in the normal and tangential directions, respectively, of the interface and, in vector notation

$$\mathbf{n}=\frac{1}{N}(-h_x\hat{i}+\hat{j}), \tag{8a}$$

$$\mathbf{t}=\frac{1}{N}(\hat{i}+h_x\hat{j}), \tag{8b}$$

where

$$N=(1+h_x^2)^{1/2}. \tag{8c}$$

The stress tensor S_{ij} is defined by

$$[S_{ij}]_g=-P\delta_{ij}+\mu_g(U_{i,j}+U_{j,i}) \tag{9a}$$

and

$$[S_{ij}]_l=-p\delta_{ij}+\mu_l(u_{i,j}+u_{j,i}), \tag{9b}$$

where U_i and u_i represent the velocities chosen to correspond to the liquid or gas flow, respectively, and δ_{ij} is the Kronecker delta. The surface tension varies with temperature according to

$$\sigma=\sigma_{\mathrm{ref}}-\gamma(T-T_{\mathrm{ref}}), \tag{10a}$$

where

$$T_{\mathrm{ref}}=\tfrac{1}{2}(T_H+T_C), \tag{10b}$$

and γ is a property of the liquid assumed to be constant; we confine our attention to liquids for which $\gamma>0$.

Because the interface position, $h(x)$, is also an unknown variable, three additional constraints are necessary to complete the mathematical formulation. Constant liquid volume must be maintained, requiring

$$\int_0^L h(x)dx=\overline{V}, \tag{11a}$$

where $\overline{V}$ equals the volume per unit length of liquid in the droplet, and, to enforce symmetry,

$$h_x=0 \quad (x=0). \tag{11b}$$

A final constraint imposes a condition where the interface contacts the bottom wall. Because our motivation for this analysis stems from experiments[5,6,11] for which the liquid droplet was affixed to a support with a sharp edge, we choose to pin the contact-line position by requiring

$$h=0 \quad (x=L). \tag{11c}$$

Lengths are scaled by L and H in the x and y directions, respectively, creating the presence of an aspect ratio, $A=H/L$, in the governing equations and interfacial boundary conditions. The remaining variables are scaled with velocities u^* and Au^*, for the x and y directions, respectively, a pressure $\mu_l u^*/HA$, a surface tension σ_{ref}, and a scale ΔT for the temperature deviation from T_{ref} where $\Delta T=T_H-T_C$ and the thermocapillary velocity scale is

$$u^*=\frac{\gamma A\Delta T}{\mu_l}. \tag{12}$$

The resulting scaled governing equations for the liquid are

$$u_x+v_y=0, \tag{13a}$$

$$\mathrm{Re}\,A(uu_x+vu_y)=-p_x+A^2u_{xx}+u_{yy}, \tag{13b}$$

$$\mathrm{Re}\,A^3(uv_x+vv_y)=-p_y+A^4v_{xx}+A^2v_{yy}, \tag{13c}$$

$$\mathrm{Ma}\,A(uT_x+vT_y)=A^2T_{xx}+T_{yy}, \tag{13d}$$

and for the gas

$$U_x+V_y=0, \tag{14a}$$

$$\rho\,\mathrm{Re}\,A(UU_x+VU_y)=-P_x+\mu(A^2U_{xx}+U_{yy}), \tag{14b}$$

$$\rho\,\mathrm{Re}\,A^3(UV_x+VV_y)=-P_y+\mu(A^4V_{xx}+A^2V_{yy}), \tag{14c}$$

$$\mathrm{Ma}\,A(U\Theta_x+V\Theta_y)=\alpha(A^2\Theta_{xx}+\Theta_{yy}), \tag{14d}$$

where

$$\rho=\frac{\rho_g}{\rho_l}, \tag{15a}$$

$$\mu=\frac{\mu_g}{\mu_l}, \tag{15b}$$

$$\alpha=\frac{\alpha_g}{\alpha_l}. \tag{15c}$$

The Reynolds number Re and Marangoni number Ma appearing in the equations are given by

$$\mathrm{Re}=\frac{\rho_l u^*H}{\mu_l}, \tag{16a}$$

$$\mathrm{Ma}=\frac{u^*H}{\alpha_l}. \tag{16b}$$

The boundary conditions become

$$u=v=0, \quad T=\tfrac{1}{2} \quad (|x|\leqslant 1, y=0), \tag{17}$$

$$U=V=0, \quad \Theta=-\tfrac{1}{2} \quad (|x|\leqslant 1, y=1), \tag{18}$$

$$u=v_x=T_x=0 \quad (x=0, y\leqslant h(x)), \tag{19}$$

$$U=V_x=\Theta_x=0 \quad (x=0, y>h(x)), \tag{20}$$

and, on the interface,

$$\begin{aligned}&-(p-P)+\frac{2A^2}{N^2}[v_y-h_xu_y+A^2h_x(h_xu_x-v_x)]\\&-\mu\frac{2A^2}{N^2}[V_y-h_xU_y+A^2h_x(h_xU_x-V_x)]\\&=\frac{A^3}{N^3\mathrm{Ca}}\left(1-\frac{\mathrm{Ca}}{A}T\right)h_{xx},\end{aligned} \tag{21a}$$

$$\begin{aligned}&\left[A^2h_x(v_y-u_x)+\frac{1}{2}(1-A^2h_x^2)(u_y+A^2v_x)\right]\\&-\mu\left[A^2h_x(V_y-U_x)+\frac{1}{2}(1-A^2h_x^2)(U_y+A^2V_x)\right]\\&=-\frac{N}{2}(T_x+h_xT_y),\end{aligned} \tag{21b}$$

$$T_x-A^2h_xT_y=\kappa(\Theta_x-A^2h_x\Theta_y), \tag{21c}$$

$$v=h_xu, \tag{21d}$$

where

$$N=(1+A^2h_x^2)^{1/2}, \quad \kappa=\frac{\kappa_g}{\kappa_l}.$$

The capillary number Ca arising in the normal stress boundary condition is defined by

$$\mathrm{Ca}=\frac{\mu_l u^*}{\sigma_{\mathrm{ref}}}. \tag{22}$$

To complete the dimensionless form of the problem, the final constraints on h become

$$\int_0^1 h\,dx=\frac{\overline{V}}{HL}=V, \tag{23a}$$

$$h_x=0 \quad (x=0), \tag{23b}$$

$$h=0 \quad (x=1). \tag{23c}$$

Our analysis treats the dimensionless equations in stream-function form, eliminating the explicit continuity statements and pressure variables. The momentum and energy balances in the two phases become

$$\mathrm{Re}\,A[(\psi_y\psi_{xyy}-\psi_x\psi_{yyy})+A^2(\psi_y\psi_{xxx}-\psi_x\psi_{xxy})] =\psi_{yyyy}+2A^2\psi_{xxyy}+A^4\psi_{xxxx}, \tag{24a}$$

$$\mathrm{Ma}\,A(\psi_yT_x-\psi_xT_y)=A^2T_{xx}+T_{yy}, \tag{24b}$$

$$\rho\,\mathrm{Re}\,A[(\Psi_y\Psi_{xyy}-\Psi_x\Psi_{yyy})+A^2(\Psi_y\Psi_{xxx}-\Psi_x\Psi_{xxy})] =\mu(\Psi_{yyyy}+2A^2\Psi_{xxyy}+A^4\Psi_{xxxx}), \tag{24c}$$

$$\mathrm{Ma}\,A(\Psi_y\Theta_x-\Psi_x\Theta_y)=\alpha(A^2\Theta_{xx}+\Theta_{yy}), \tag{24d}$$

where ψ and Ψ designate the stream function in the liquid and gas, respectively. The kinematic constraints are then imposed by requiring

$$\psi=\psi_y=0 \quad \text{at } y=0, \tag{25a}$$

$$\Psi=\Psi_y=0 \quad \text{at } y=1, \tag{25b}$$

$$\psi=\Psi=0, \quad \text{and } \psi_y=\Psi_y \quad \text{at } y=h(x), \tag{26}$$

and the normal- and shear-stress boundary conditions become

$$-(p-P)+\frac{2A^2}{N^2}[-\psi_{xy}-h_x\psi_{yy}+A^2h_x(h_x\psi_{yx}+\psi_{xx})] -\mu\frac{2A^2}{N^2}[-\Psi_{xy}-h_x\Psi_{yy}+A^2h_x(h_x\Psi_{yx}+\Psi_{xx})] =\frac{A^3}{N^3\,\mathrm{Ca}}\left(1-\frac{\mathrm{Ca}}{A}T\right)h_{xx}, \tag{27a}$$

$$\left[A^2h_x(-\psi_{xy}-\psi_{yx})+\frac{1}{2}(1-A^2h_x^2)(\psi_{yy}-A^2\psi_{xx})\right] -\mu\left[A^2h_x(-\Psi_{xy}-\Psi_{yx})+\frac{1}{2}(1-A^2h_x^2)(\Psi_{yy} -A^2\Psi_{xx})\right]=-\frac{N}{2}(T_x+h_xT_y). \tag{27b}$$

Restricting attention to a thin-film analysis, we seek an asymptotic solution in terms of A as the small parameter. Thus, the analysis is restricted to the situation where $H \ll L$, implying a thin gap and a droplet that behaves as a thin film. The expansions for the interface position, as well as the gas and liquid stream-function, temperature, and pressure fields represented by

$$h=h_0(x)+h_1(x)A+O(A^2), \tag{28a}$$

$$\psi=\psi_0(x,y)+\psi_1(x,y)A+O(A^2), \tag{28b}$$

$$p=p_0(x,y)+p_1(x,y)A+O(A^2), \tag{28c}$$

$$T=T_0(x,y)+T_1(x,y)A+O(A^2), \tag{28d}$$

$$\Psi=\Psi_0(x,y)+\Psi_1(x,y)A+O(A^2), \tag{28e}$$

$$P=P_0(x,y)+P_1(x,y)A+O(A^2), \tag{28f}$$

$$\Theta=\Theta_0(x,y)+\Theta_1(x,y)A+O(A^2), \tag{28g}$$

are substituted into the problem defined by Eqs. (23)–(27). The subsequent problems governing the $O(1)$ and $O(A)$ components of these expansions are referred to as the leading- and first-order problems, respectively. The dimensionless parameters in the analysis are assumed to be of orders

$$\mathrm{Ca}=O(A^3), \tag{29a}$$

$$\mathrm{Ma}=O(A), \tag{29b}$$

$$\mathrm{Re}=O(1) \tag{29c}$$

with

$$\rho,\mu,\alpha, \quad \text{and } \kappa=O(1). \tag{30}$$

The choice $\mathrm{Ca}=O(A^3)$ is critical to the development of an asymptotic solution since other choices lead to mathematical obstacles. For $\mathrm{Ca}=O(A^2)$ and larger, the leading order pressure fields are constant resulting in a static leading-order flow field, while $\mathrm{Ca}=O(A^4)$ or smaller, meaning $\mathrm{Ca}=o(A^4)$, results in a flat interface to leading order. In the latter case, an interface with zero curvature is subsequently found within the then necessary boundary layer near the contact line which prohibits matching to the outer flow. The choice in our case of $\mathrm{Ca}=O(A^3)$ results in a two-dimensional leading-order flow field with a curved interface. With interface curvature, the contact-line condition is satisfied without the presence of a boundary layer. The two-dimensional flow field permits recirculation in the absence of boundary layers. In the thermocapillary slot flow problem of Sen and Davis[12] with an $O(A^4)$ capillary number, the leading-order solutions contain a flat interface and one-dimensional core flow requiring boundary layers at the end-walls to allow recirculation. Our lack of a one-dimensional

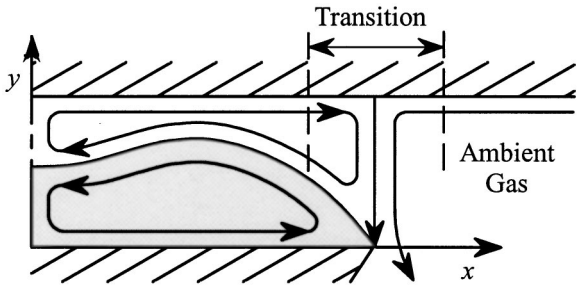

FIG. 2. Gas flow transition layer.

core flow can be explained by recognizing some physical characteristics of the problem considered herein. In the problem of Sen and Davis, a uniform interfacial-temperature gradient spans the length of the leading-order interface which permits a fully developed interior flow. In the present droplet, the interfacial-temperature gradient decays to zero at the center of the droplet as required by Eq. (19). Thus, the leading-order bulk fluid motion must also decay, never allowing a fully developed flow. A reexamination of the thermocapillary slot flow problem with $\mathrm{Ca}=O(A^3)$ by Sen[13] found an entirely two-dimensional leading-order flow although boundary layers remained necessary.

Consistent with lubrication theory, the nature of the asymptotic, thin-film analysis neglects terms in the leading- and first-order governing equations that involve derivatives in the direction along the gap length. The resulting flow and temperature conditions in the solutions at $x=0,1$ dependent implicitly upon the end constraints on $h(x)$. It can be shown that imposing symmetry on the interface at $x=0$ with Eq. (23b) also enforces the kinematic requirement of symmetry on the velocity and thermal fields in both fluid phases. Without a kinematically prescribed boundary for the gas at $x=1$, the resulting conditions found in the gas there cannot be substantiated. The pinned-contact-line condition of Eq. (23c) causes a segregating vertical streamline through the contact line where $\psi=0$ as shown in Fig. 2, implying complete recirculation above the droplet and forbidding ambient gas entrainment. The solution is not found to be symmetric about this segregating streamline in that neither v_x nor Θ_x equals zero. Segregating the flow abruptly at $x=1$ lacks physical rationale even at leading order while neglecting inertia. The shear stress induced on the interface drives flow in the transition region near the contact line lowering the local gas pressure precisely where the ambient gas remains accessible. Incorporating a transition layer matching the lubricating flow above the droplet to the ambient gas conditions would allow the implementation of the appropriate physics governing entrainment. Ambient conditions will then influence the flow in the transition region with thickness of $O(A)$ or smaller, but cannot impact the innermost lubrication flow near the dimple. Since, in the present work we focus on investigating the presence of the dimple at the center of the droplet, resolving the gas transition layer at $x=1$ for a particular ambient flow is not necessary. The recirculation of the gas flow near the contact line in the solutions that follow is physically unrealistic and could be corrected when warranted by resolving the transition layer.

The choice for the Marangoni number to be $O(A)$ removes the influence of convection so that the thermal field is nearly pure conduction up to first order and thus independent of the value of Ma and α. Avoiding the complications of convection until second order allows a simple and direct means to investigate the role of inertia. Thus, the present effort represents only a first step into a complete investigation of the possible consequences of inertia.

The Reynolds number, representing the relative importance of inertial and viscous forces, is crucial to our investigation into droplet deformation. A Reynolds number of $O(1)$ or smaller in A ensures that viscosity dominates the leading-order flow as lubrication theory dictates, so that the leading-order flow does not depend on Re or ρ. In the case of $\mathrm{Re}=O(1)$, the influence of inertia is observed immediately in the first-order correction. Choosing $\mathrm{Re}=O(A)$ or smaller simply delays the inclusion of inertia to smaller orders.

Although not appearing in the problem definition, the orders of Ma and Re implicitly dictate the Prandtl number Pr to be $O(A)$, since $\mathrm{Pr}=\mathrm{Ma}/\mathrm{Re}$.

A. The leading-order problem

Considering A as an independent parameter, a problem corresponding to each order expansions (28a)–(28g) can be determined. The leading-order problem consists of the governing equations

$$\psi_{0yyyy}=0, \tag{31a}$$

$$T_{0yy}=0, \tag{31b}$$

$$\Psi_{0yyyy}=0, \tag{32a}$$

$$\Theta_{0yy}=0, \tag{32b}$$

subject to boundary conditions

$$\psi_{0y}=\psi_0=0, \quad \text{and} \quad T_0=\tfrac{1}{2} \quad (y=0), \tag{33}$$

$$\Psi_{0y}=\Psi_0=0, \quad \text{and} \quad \Theta_0=-\tfrac{1}{2} \quad (y=1), \tag{34}$$

and on the interface where $y=h_0$,

$$\psi_0=\Psi_0=0, \quad \psi_{0y}=\Psi_{0y}, \tag{35a}$$

$$\psi_{0yy}-\mu\Psi_{0yy}=T_{0x}+h_{0x}T_{0y}, \tag{35b}$$

$$P_0-p_0=\frac{h_{0xx}}{C}, \tag{35c}$$

$$T_{0y}=\kappa\Theta_{0y}, \tag{35d}$$

$$T_0=\Theta_0, \tag{35e}$$

where C arises when enforcing the order of Ca by using $\mathrm{Ca}=CA^3$. To complete the problem definition,

$$\int_0^1 h_0 dx=\overline{V}, \tag{36a}$$

$$h_{0x}=0 \quad (x=0), \tag{36b}$$

$$h_0=0 \quad (x=1), \tag{36c}$$

constrain the unknown interface position $h_0(x)$.

Direct integration of Eqs. (31) and (32) and application of the boundary conditions, (33), (34), (35a), (35b), (35d), and (35e) leads to

$$\psi_0=\frac{-\kappa(h_0-1)h_{0x}}{4M_0K_0^2h_0}(y^3-h_0y^2), \tag{37a}$$

$$\Psi_0=\frac{-\kappa h_0h_{0x}}{4M_0K_0^2(h_0-1)}[y^3-1-(h_0+2)(y^2-1) +(2h_0+1)(y-1)], \tag{37b}$$

$$T_0=\frac{-\kappa}{K_0}y+\frac{1}{2}, \tag{37c}$$

$$\Theta_0=\frac{-1}{K_0}(y-1)-\frac{1}{2}, \tag{37d}$$

where $M_0=h_0(\mu-1)+1$ and $K_0=h_0(\kappa-1)+1$, providing an analytical solution for the flow and temperature fields in terms of a yet unknown leading-order interface position $h_0(x)$. The leading-order momentum-balance equations (13b), (13c), (14b), and (14c) then show that

$$P_{0y}=p_{0y}=0, \tag{38a}$$

$$p_{0x}=\frac{-3(h_0-1)\kappa h_{0x}}{2M_0K_0^2h_0}, \tag{38b}$$

$$P_{0x}=\frac{-3\mu\kappa h_0h_{0x}}{2M_0K_0^2(h_0-1)}. \tag{38c}$$

Differentiating Eq. (35c) with respect to the x direction and substituting for the pressure fields yields

$$h_0(h_0-1)M_0K_0^2h_{0xxx}+\tfrac{3}{2}C\kappa(h_0M_0+h_0-1)h_{0x}=0, \tag{39}$$

which governs the leading order interface position subject to the auxiliary conditions of Eqs. (36a)–(36c). The nonlinear system composed of Eqs. (39) and (36a)–(36c) is solved numerically with a second-order-accurate central-differencing scheme on a uniformly spaced grid. For convenience, a second-order-accurate backward-difference approximation is employed at a single node neighboring $x=1$. An iterative computation procedure imposes either a circular-arc interface shape as assumed by Wood[20] or a previously computed solution in nearby parameter space for an initial guess of h_0.

B. The first-order problem

The first-order problem in the case with $\mathrm{Re}=O(1)$ is defined by the governing equations

$$\mathrm{Re}(\psi_{0y}\psi_{0xy}-\psi_{0x}\psi_{0yy})_y=\psi_{1yyyy}, \tag{40a}$$

$$T_{1yy}=0, \tag{40b}$$

$$\rho\,\mathrm{Re}(\Psi_{0y}\Psi_{0xy}-\Psi_{0x}\Psi_{0yy})_y=\mu\Psi_{1yyyy}, \tag{41a}$$

$$\Theta_{1yy}=0, \tag{41b}$$

with boundary conditions

$$\psi_{1y}=\psi_1=0, \quad \text{and} \quad T_1=0 \quad (y=0), \tag{42}$$

$$\Psi_{1y}=\Psi_1=0, \quad \text{and} \quad \Theta_1=0 \quad (y=1), \tag{43}$$

required to satisfy no slip, no penetration, and isothermal plates. The first-order version of the interfacial boundary conditions is given by

$$\psi_1=\Psi_1=\frac{-\kappa(h_0-1)h_0h_{0x}}{4M_0K_0^2}h_1, \tag{44a}$$

$$\frac{\kappa h_{0x}}{M_0K_0^2}h_1+\psi_{1y}=\Psi_{1y}, \tag{44b}$$

$$\psi_{1yy}-\mu\Psi_{1yy}=-T_{1x}-h_{0x}T_{1y}-T_{0y}h_{1x}-G_0h_1, \tag{44c}$$

$$P_1-p_1=\frac{h_{1xx}}{C}, \tag{44d}$$

$$T_{1y}=\kappa\Theta_{1y}, \tag{44e}$$

and

$$T_1=\Theta_1+\frac{(\kappa-1)h_1}{K_0}, \tag{44f}$$

where

$$G_0=\frac{T_{0x}}{h_0}+\frac{3\kappa}{2}\left(\frac{h_0-1}{h_0}-\frac{\mu h_0}{h_0-1}\right)\frac{(h_0-1)h_{0x}}{h_0M_0K_0^2}$$

apply at $y=h_0$. Finally, the correction of the interface position is constrained by

$$\int_0^1 h_1dx=0, \quad h_{1x}=0 \quad (x=0), \quad \text{and} \quad h_1=0 \quad (x=1). \tag{45}$$

We solve the first-order problem with the same methodology applied to the leading order problem. The governing equations (40b) and (41b) and auxiliary conditions (42), (43), and (44e), (44f) provide

$$T_1=\frac{\kappa(\kappa-1)h_1}{K_0^2}y \tag{46}$$

and

$$\Theta_1=\frac{(\kappa-1)h_1}{K_0^2}(y-1) \tag{47}$$

for the correction to the temperature field in terms of the unknown interface correction h_1. Equations (40a) and (41a) imply solutions of the form

$$\psi_1=\mathrm{Re}\int\int\int(\psi_{0y}\psi_{0xy}-\psi_{0x}\psi_{0yy})dy^3 +\frac{1}{6}C_1(x)y^3+\frac{1}{2}C_2(x)y^2+C_3(x)y+C_4(x), \tag{48}$$

and

$$\Psi_1=\frac{\rho}{\mu}\mathrm{Re}\int\int\int(\Psi_{0y}\Psi_{0xy}-\Psi_{0x}\Psi_{0yy})dy^3 + \frac{1}{6}B_1(x)y^3+\frac{1}{2}B_2(x)y^2+B_3(x)y+B_4(x), \quad (49)$$

where $C_i(x)$ and $B_j(x)$ represent arbitrary functions due to the integration over the y variable. These eight functions have analytical expressions in terms of h_0 and h_1 dictated by the auxiliary conditions (42), (43), (44a)–(44c). The first-order normal-stress boundary condition (44d) then governs the interface correction h_1 and takes the form

$$\mu B_1(x)-C_1(x)=\frac{h_{1xxx}}{C}, \quad (50)$$

where $B_1(x)$ and $C_1(x)$ are found to be linear operators on h_1 and h_{1x}. The resulting nonhomogeneous linear equation is solved with the finite-difference techniques employed for the leading-order problem.

Considering $\mathrm{Re}=O(A)$ instead would remove the consideration of inertia from the first-order problem resulting in a linear, but homogeneous equation. The first-order correction with a relaxed volume constraint could then be specified to within the multiplication of an arbitrary constant implying a unique interface shape independent of volume. The net volume of the correction must also be a multiple of this constant. Because maintaining a fixed liquid volume, independent of A, necessitates a net zero volume constraint for each interface correction, a trivial solution of zero for the interface correction cannot be avoided. The governing equation of the second-order problem would be nonhomogeneous due to the now present inertia terms permitting a nonzero $O(A^2)$ correction.

These leading- and first-order problems for $\mathrm{Re}=O(A)$ also apply for the case of $\mathrm{Re}=O(A^2)$ and smaller. The second-order correction for the case with $\mathrm{Re}=O(A^2)$, which remains viscously dominated, is not necessarily zero as is the viscously dominated first-order correction, and may lead to the formation of a dimple. Complications arise with x- and y-direction derivatives now significant in the momentum balance. The flow-field correction might then be solved numerically as was done by Sen and Davis.[12]

To gain insight regarding the importance of inertia in the dimple formation, we present solutions to the simpler problem of $\mathrm{Re}=O(1)$ to incorporate inertia in the first correction. We are able to show then how the presence of inertia influences the formation of a dimple but cannot preclude the possibility of a dimple shape due to an $O(A^2)$ viscous effect. Furthermore, the choices of $\mathrm{Re}=O(1)$ and $\mathrm{Ma}=O(A)$ restrict the Prandtl number to $O(A)$ for the solutions presented herein.

III. RESULTS

The results to be presented begin with three cases: (1) a solution for a single set of parameters; (2) a case identical to (1) but with a larger liquid volume fraction; and (3) a case identical to (1) with a smaller value for the thermal-conductivity ratio. These are followed by a series of investigations into the influence of defined parameters on droplet shape. The following parameter values define case (1):

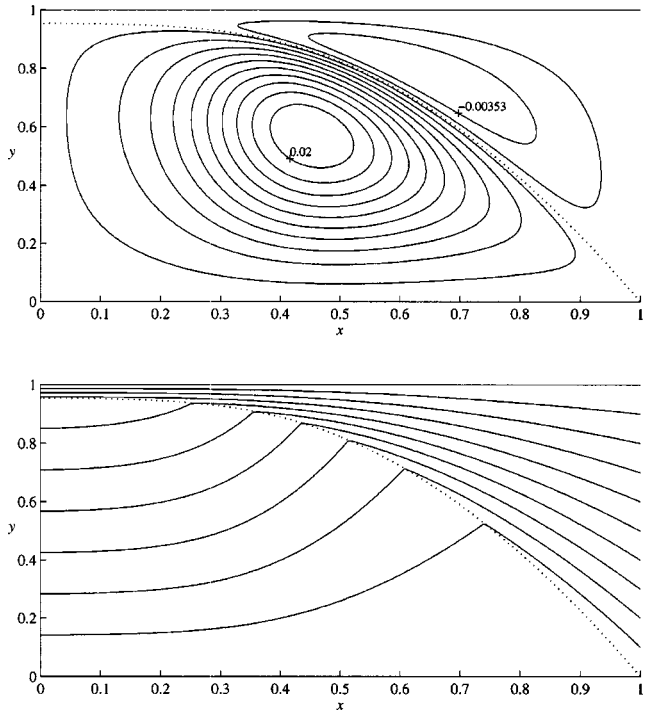

FIG. 3. Leading-order streamlines and isotherms for case (1).

$$V=0.7, \quad C=1, \quad \mu=0.1, \quad \kappa=0.1,$$

$$\rho=0.001, \quad \mathrm{Re}=5000.$$

The two parameters ρ and Re impact the role of inertia and thus only influence the correction. The relatively large value for Re serves only to provide a distinguishable presentation of the droplet-shape correction.

The viscously dominated leading-order solution for case (1) is given in Fig. 3, which shows both streamlines and isotherms. The dotted curve represents the droplet interface; contour values are equally spaced. These solutions are relevant in the limit as A approaches zero which corresponds physically to the limit as L approaches infinity implying a long, flat droplet. The streamlines show a single-cell flow structure in the liquid below the interface and another in the gas above. The leading-order flow satisfies the kinematic boundary condition on the interface [Eq. (26)] identically. The complete recirculation of the gas above the droplet is a consequence of our choice not to resolve the transition layer near $x=1$. The isotherms show the pure-conduction state with a discontinuous slope in the contours at the interface due to the change in thermal conductivity since $\kappa\neq 1$. Symmetry in the temperature field can be observed at $x=0$, while the nonzero heat addition at $x=1$ is not meaningful in the absence of a transition-layer correction.

The interface-temperature gradient that drives the flow decays to zero as x approaches zero as dictated by Eq. (19). With a negligible driving mechanism near $x=0$ and no inertia, the flow simply dissipates in the interior where the dimple is expected to form. To search for a possible dimpled shape at leading order, we examine case (2), increasing V to

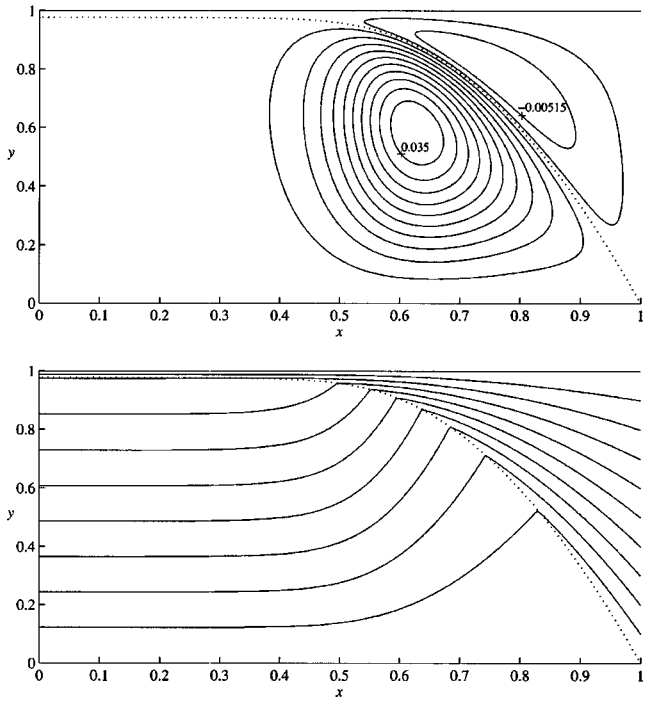

FIG. 4. Leading-order streamlines and isotherms for case (2).

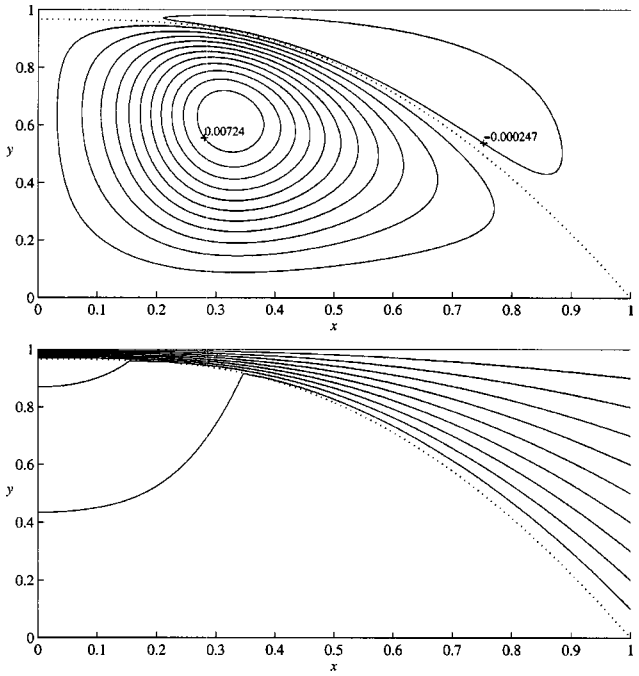

FIG. 5. Leading-order streamlines and isotherms for case (3).

simulate an attempt to force the droplet to wet the wall. Figure 4 shows the leading-order solution with V set to 0.8. Recall that the present analysis does not permit wetting and thus this solution may not correspond to a realizable scenario. Still, under these conditions of extreme droplet deformation, we find that, rather than prompting a dimple, the impact on the interior flow lessens. In a second attempt to find a leading-order dimple, for case (3), we decrease the value of κ with the intent to redistribute the driving interfacial temperature gradient more toward the center of the droplet. The resulting solution shown in Fig. 5 lacks an interior region of purely dissipative flow, and, although the droplet shape is significantly altered, the interface curvature characteristic of a dimple remains absent. Comparing the results in Figs. 3–5, we notice that the location of the center of the flow cell follows that of the driving mechanism, i.e., the region with a relatively larger interfacial temperature gradient. Finally, a complete parameter search reveals no evidence of the possibility for an $O(1)$ dimpled shape. The parameter influences on droplet shape are discussed in the following.

The first-order corrections for case (1) are shown in Figs. 6 and 7. The droplet-shape correction, h_1 is shown in Fig. 6(a) along with the leading-order shape and the resulting corrected shape for two values of A. A dimpled shape appears as a result of the correction. The leading- and first-order versions of the normal-stress boundary condition [Eqs. (35c) and (44d)] specify the consequential pressure difference across the interface shown in Fig. 6(b). The pressure field in each phase has only an x-direction dependence to these orders in A where the interface curvature dictates the pressure difference. Comparing Figs. 6(a) and 6(b) reveals the necessary positive pressure difference where the dimple forms and appropriate correspondence between the inflection points in the droplet shape and zero values in the pressure difference. The first-order correction of the pressure difference P_1-p_1 reveals a local maximum located near $x=0.25$, observed to correspond with a local maximum in the interface curvature, and a second, smaller local maximum located near $x=0.5$. This second local maximum shows the first evidence of interface curvature near $x=0.5$ which is shown to be more discernible in later cases discussed in the following.

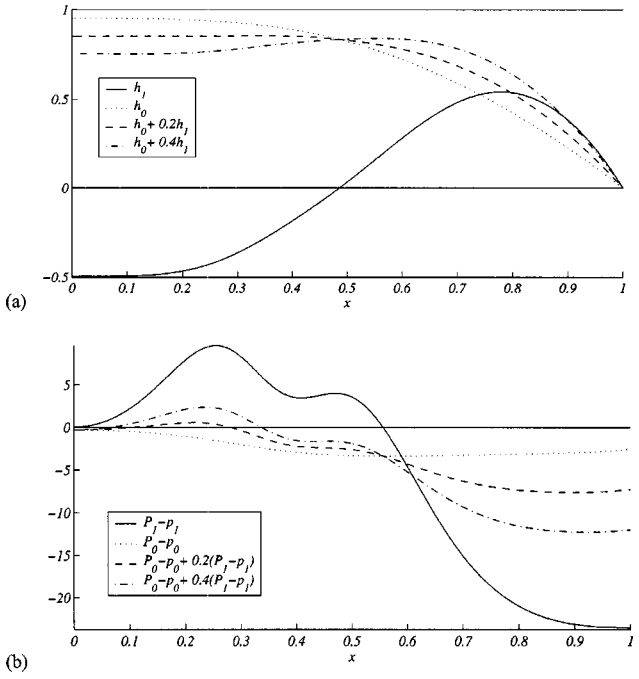

FIG. 6. Interface correction for case (1): (a) droplet-shape, (b) resulting interfacial pressure difference.

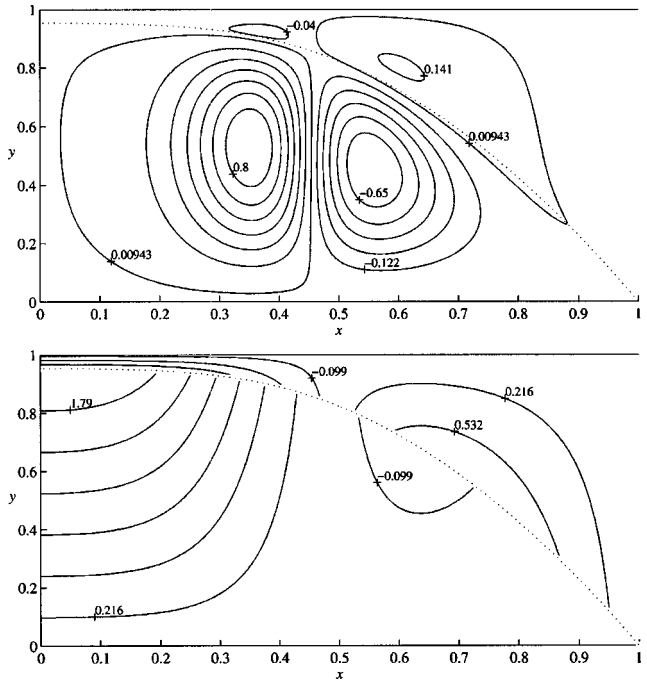

FIG. 7. Stream-function and isotherm corrections for case (1).

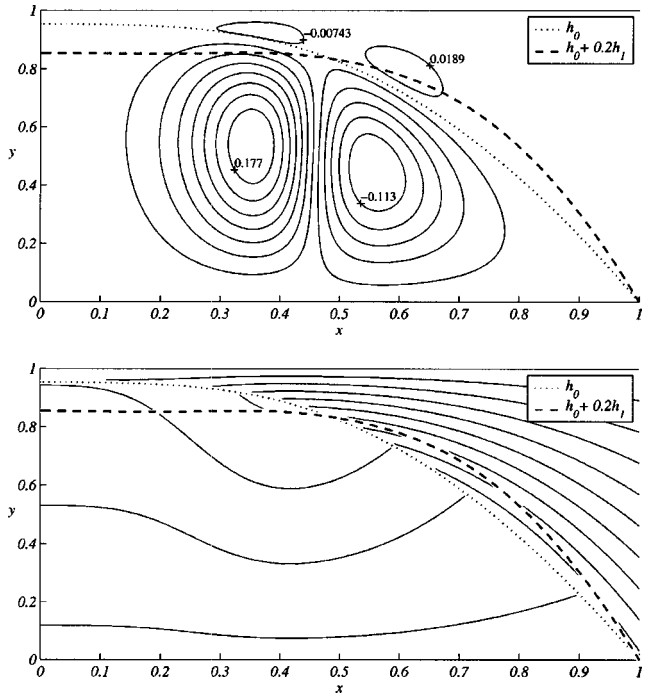

FIG. 8. Streamlines and isotherms corrected to $O(A)$ for case (1).

Figure 7 presents the streamlines and isotherms of the correction. In these graphs, the leading-order interface position distinguishes the gas and liquid phases although the interface correction is nonzero. This presentation is chosen due to the nature of the asymptotics employed, which requires the solution corrections to be independent of A [as shown in Eqs. (28a)–(28g)]. The streamline correction consists of a two-cell flow structure in the liquid and again in the gas. Notice that the amplitude of the stream-function correction is an order of magnitude larger than the leading-order stream function while the droplet-shape correction remains comparable to the leading-order droplet shape. This can be expected since Ca is $O(A^3)$ while Re is $O(1)$. The isotherms deviate from pure conduction due to the implicit influence of the leading-order flow field on the temperature correction.

The resulting flow and temperature fields corrected to $O(A)$ are shown in Fig. 8, for the choice $A=0.2$. The fluid phases remain distinguished with the leading-order shape marked by a dotted line. The dashed line indicates the corrected droplet shape for $A=0.2$. The streamlines, showing the dual-cell structure of the correction in each phase, are dominated by the correction as was found necessary to present a distinguishable adjustment of the leading-order shape for reasons discussed above. The leading-order temperature field remains evident in the corrected flow. The Marangoni number of $O(A)$ delays the appearance of the convection terms in the energy balance until $O(A^2)$ so that the next correction to the thermal field would be expected to dominate as is the case of the first-order stream function.

Figure 9 considers the influence of C (recall $\mathrm{Ca}=CA^3$) with remaining parameters as specified for case (1). Increasing C simulates a reduction in surface tension and consequently an increased surface flexibility. Varying C from 0.2 to 10 increases the leading-order droplet deformation due to the presence of the upper wall as shown in Fig. 9(a). The gap width between the droplet and the wall increases but with no evidence of the curvature necessary for a dimple. The dimple influence of the interface correction increases as shown in Fig. 9(b). For sufficiently high values of C, a critical point of zero slope is found to develop away from $x=0$. This influence can be seen in the corrected droplet shapes of Fig. 9(c). The increase in interface curvature near this critical point is associated with an increase in the local pressure difference across the interface which for the case of $C=1$ appears as the local maximum near $x=0.5$ in Fig. 6(b) although the consequential interface curvature is not visually distinguishable as in the cases with $C=5$ or 10. Given the thin-film restriction of this analysis, the influence of inertia via the correction decays far into the interior.

The influence of liquid volume V is similar to that of C as can be seen in Fig. 10, the primary difference being that increasing V decreases the gap width contrary to the behavior with varying C. Increasing V emphasizes droplet deformation due to the wall in a similar fashion as increasing C; the region of zero curvature about the center of the leading-order droplet shape expands. Furthermore, the interface corrections given in Fig. 10(b) show, although on a different scale, shapes similar to those found when investigating the influence of C even in the formation of a critical point away from $x=0$ for the larger volumes considered. Through the implicit dependence of the correction on the leading-order flow, C and V remain independent parameters in the first-order problem despite their similar influences. The corrected droplet shapes computed for increasing volumes show little impact on droplet height in the interior due to the canceling influences of the leading-order shape and the correction while, away from the interior, the growth of a bulge is ob-

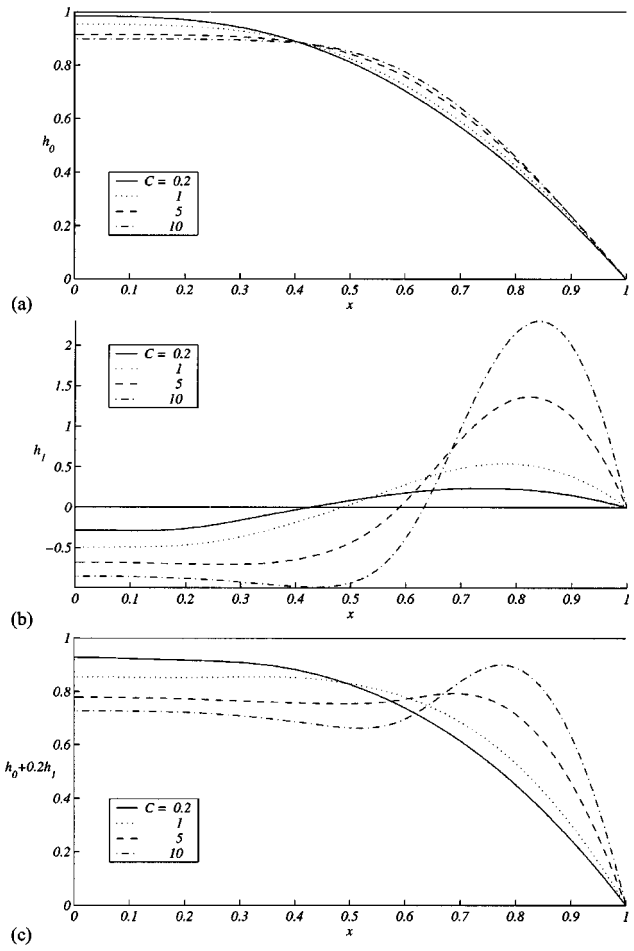

FIG. 9. Influence of C on droplet shape with remaining parameters values corresponding to case (1): (a) leading-order solution, (b) first-order correction, (c) solution corrected to $O(A)$.

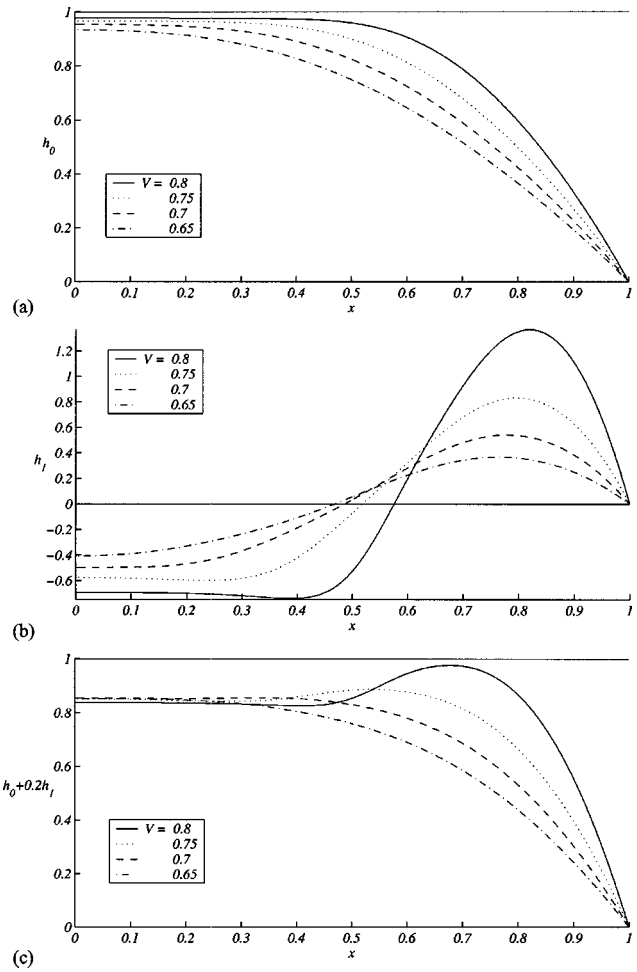

FIG. 10. Influence of V on droplet shape with remaining parameters values corresponding to case (1): (a) leading-order solution, (b) first-order correction, (c) solution corrected to $O(A)$.

served. The consequence of the bulge shape is again to form a dimple.

The influence of varying μ and thus the viscosity of the gas relative to that of the liquid is presented in Fig. 11 and reveals the role of viscosity in the lubricating layer. Figure 11(a) shows that increasing μ increases the leading-order gap width. The equations become stiff for values of μ below 0.01. The corrections in Fig. 11(b) show the dimple shapes for small values of μ with an amplitude that decays to zero as μ increases. The role of gas viscosity contributes to maintaining droplet separation from the opposing wall but reduces the impact of inertia in the correction.

The density ratio, ρ, influences the correction as shown in Fig. 12. Decreasing ρ and thus the density of the gas relative to that of the liquid reduces the dimpling influence of the correction. However, in the limit as ρ approaches zero, the correction approaches a nonzero amplitude corresponding approximately to the case with $\rho=0.01$. The inertia in both the liquid and gas influence the size of a dimple, and a dimple exists in the absence of inertia in the gas.

With the Reynolds number chosen to be $O(1)$, the value of Re appears as a scale of the nonhomogeneous term in the linear differential equations [Eqs. (40a) and (41a)] governing the flow-field correction. The solution can consequently be written in our case as a single solution scaled by Re such that if ψ corresponds to Re=1, then $\psi=\mathrm{Re}\,\psi$ provides a solution for any fixed value of Re. In the limit as Re approaches zero, the correction approaches zero and at the same rate, the first-order problem definition approaches that corresponding to the Re$=O(A)$ case. We can again conclude that an $O(A)$ solution does not exist without the consideration of inertia.

IV. CONCLUSIONS

A lubrication analysis has been performed for a thermocapillary-driven nonwetting droplet focusing on the respective influences of viscosity and inertia. The present analysis neglects the effects of gravity and considers a two-dimensional, symmetric liquid droplet coupled at the surface with a non-passive gas. Although the lubricating fluid is referred to as a gas, the results found are equally applicable to immiscible-liquid pairs.

Dimensionless parameters are specified as fixed orders of the aspect ratio. Due to the curved droplet shape and nonuniform interfacial temperature gradient, a capillary number of $O(A^3)$ was found necessary to facilitate analytical results. The order of the Marangoni number remained fixed at $O(A)$ to delay the influence of convection on the thermal field and allow the analysis to focus on the roles of viscosity and in-

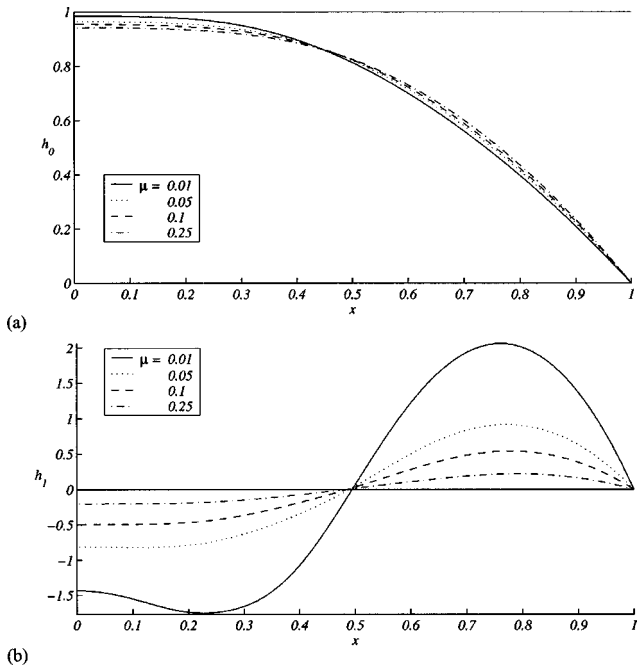

FIG. 11. Influence of μ on droplet shape with remaining parameters values corresponding to case (1): (a) leading-order solution, (b) first-order correction.

ertia. The consequences of various choices for the order of the Reynolds number are discussed and results are presented for the case with the Reynolds number of $O(1)$.

The complete recirculation within the gas flow above the droplet in the presented solutions is a consequence of a neglected transition layer in the gas that would permit matching the lubricating layer to ambient gas conditions. With concerns focused at the center of the droplet, we chose to not resolve the transition layer that we reason would have little, if any effect on the observed dimpling.

The $O(1)$ influence of gas viscosity contributes to maintaining a nonwetting droplet and the $O(A)$ influence of inertia creates a dimpled shape in the droplet surface. The $O(1)$ influence of viscosity does not reveal a dimple and, after a limited search over parameter space, provides no evidence for possible regimes allowing an $O(1)$ dimple. The parameter influences considered include the capillary number, the liquid volume fraction, the viscosity ratio, the density ratio and the Reynolds number.

Additionally, viscosity has no $O(A)$ impact in that this correction without inertia is shown to be zero. The $O(A^2)$ influence of viscosity alone warrants consideration although it is not investigated herein. Thus, we cannot conclude that inertia provides the only means for the existence of a dimple, although if viscosity serves as a contributor its influence will be $O(A^2)$ or smaller.

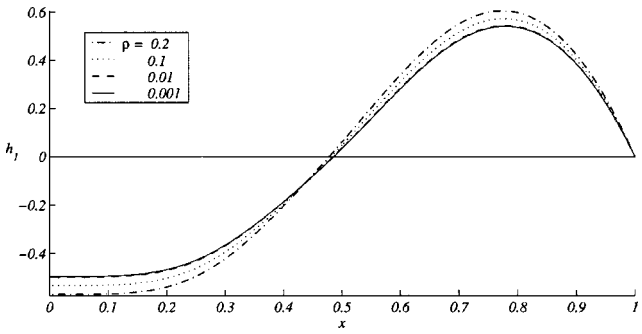

FIG. 12. Influence of ρ on droplet shape with remaining parameters values corresponding to case (1).

ACKNOWLEDGMENTS

G.P.N. and A.M.W. acknowledge support received from NASA's Office of Biological and Physical Research and L.B.S.S. thanks NASA for support received through a NASA/ASEE Summer Faculty Fellowship at the Microgravity Fluid Physics Branch, Glenn Research Center. We thank Professor M. K. Smith for many helpful discussions during the course of this research.

[1] L. Rayleigh, "On the capillary phenomena of jets," Proc. R. Soc. London, Ser. A **29**, 71 (1879).
[2] L. Rayleigh, "Further observations upon liquid jets, in continuation of those recorded in the Royal Society's Proceedings for March and May, 1879," Proc. R. Soc. London **34**, 130 (1882).
[3] L. Rayleigh, "Investigations in capillarity:—the size of drops.—the liberation of gas from supersaturated solutions.—colliding jets.—the tension of contaminated water surfaces.—a curious observation," Philos. Mag. **48**, 321 (1899).
[4] O. Reynolds, "On drops floating on the surface of water," Chem. News **44**, 211 (1881).
[5] P. Dell'Aversana, J. R. Banavar, and J. Koplik, "Suppression of coalescence by shear and temperature gradients," Phys. Fluids **8**, 15 (1996).
[6] P. Dell'Aversana, V. Tontodonato, and L. Carotenuto, "Suppression of coalescence and wetting: The shape of the interstitial film," Phys. Fluids **9**, 2475 (1997).
[7] P. Dell'Aversana and G. P. Neitzel, "When liquids stay dry," Phys. Today **51** (1), 38 (1998).
[8] R. Monti and R. Savino, "Correlation between experimental results and numerical solutions of the Navier–Stokes problem for noncoalescing liquid drops with Marangoni effects," Phys. Fluids **9**, 260 (1997).
[9] R. Monti, R. Savino, and S. Tempesta, "Wetting prevention by thermal Marangoni effect. Experimental and numerical results," Eur. J. Mech. B/Fluids **17**, 51 (1998).
[10] G. P. Neitzel and P. Dell'Aversana, "Noncoalescence and nonwetting behavior of liquids," Annu. Rev. Fluid Mech. **34**, 267 (2002).
[11] J. Nalevanko, "Design of an apparatus for investigation of 2-D liquid drop non-coalescence," M.S. thesis, Georgia Institute of Technology, 1997.
[12] A. K. Sen and S. H. Davis, "Steady thermocapillary flows in two-dimensional slots," J. Fluid Mech. **121**, 163 (1982).
[13] A. K. Sen, "Thermocapillary convection in a rectangular cavity with a deformable interface," Phys. Fluids **29**, 3881 (1986).
[14] P. Ehrhard and S. H. Davis, "Non-isothermal spreading of liquid drops on horizontal plates," J. Fluid Mech. **229**, 365 (1991).
[15] S. W. Benintendi and M. K. Smith, "The spreading of a non-isothermal liquid droplet," Phys. Fluids **11**, 982 (1999).
[16] M. K. Smith, "Thermocapillary migration of a two-dimensional droplet on a solid surface," J. Fluid Mech. **294**, 209 (1995).
[17] S. J. Van Hook, M. F. Schatz, J. B. Swift, W. D. McCormick, and H. L. Swinney, "Long-wave instability in surface-tension-driven Bénard convection," Phys. Rev. Lett. **75**, 4397 (1995).
[18] A. A. Golovin, A. A. Nepomnyashchy, and L. M. Pismen, "Nonlinear evolution and secondary instabilities of Marangoni convection in a liquid gas system with deformable interface," J. Fluid Mech. **341**, 317 (1997).
[19] S. J. Van Hook, M. F. Schatz, J. B. Swift, W. D. McCormick, and H. L. Swinney, "Long-wavelength surface-tension-driven Bénard convection: Experiment and theory," J. Fluid Mech. **345**, 45 (1997).
[20] A. M. Wood, "Steady thermocapillary flow between a non-wetting liquid droplet and a solid surface," M.S. thesis, Georgia Institute of Technology, 2000.